NANO MICRO small
www.small-journal.com

Performance of Preformed Au/Cu Nanoclusters Deposited on MgO Powders in the Catalytic Reduction of 4-Nitrophenol in Solution

*Rongsheng Cai, Peter R. Ellis, Jinlong Yin, Jian Liu, Christopher M. Brown, Ross Griffin, Guojing Chang, Dongjiang Yang, Jun Ren, Kevin Cooke, Peter T. Bishop, Wolfgang Theis, and Richard E. Palmer**

The deposition of preformed nanocluster beams onto suitable supports represents a new paradigm for the precise preparation of heterogeneous catalysts. The performance of the new materials must be validated in model catalytic reactions. It is shown that gold/copper (Au/Cu) nanoalloy clusters (nanoparticles) of variable composition, created by sputtering and gas phase condensation before deposition onto magnesium oxide powders, are highly active for the catalytic reduction of 4-nitrophenol in solution at room temperature. Au/Cu bimetallic clusters offer decreased catalyst cost compared with pure Au and the prospect of beneficial synergistic effects. Energy-dispersive X-ray spectroscopy coupled with aberration-corrected scanning transmission electron microscopy imaging confirms that the Au/Cu bimetallic clusters have an alloy structure with Au and Cu atoms randomly located. Reaction rate analysis shows that catalysts with approximately equal amounts of Au and Cu are much more active than Au-rich or Cu-rich clusters. Thus, the interplay between the Au and Cu atoms at the cluster surface appears to enhance the catalytic activity substantially, consistent with model density functional theory calculations of molecular binding energies. Moreover, the physically deposited clusters with Au/Cu ratio close to 1 show a 25-fold higher activity than an Au/Cu reference sample made by chemical impregnation.

1. Introduction

Cluster beam deposition is a new method to prepare heterogeneous catalysts for research and development, in which atomic clusters (nanoparticles) of tunable size typically below 10 nm are pre-assembled into a beam and then deposited in a vacuum chamber onto the catalyst support.[1–4] Potential advantages of the approach include the absence of solvent and effluent in the catalyst synthesis; control of cluster size, composition, and morphology; and the absence of ligands compared with colloidal routes.[5–8] However, the technique is at an early stage,[9] most especially where catalytic behavior under realistic reaction conditions is concerned. Thus, there is an urgent need to validate the performance of this new class of nanomaterials in a series of model chemical transformations, and compare their behavior with catalysts prepared by more traditional and well-established routes. In this work, we report a first investigation of a solution phase transformation performed by nanoalloy catalysts prepared by cluster beam deposition.

The discovery of the catalytic activity of gold (Au) nanoparticles for low-temperature oxidation of carbon monooxide (CO) provoked an explosion of interest in gold catalysis.[10,11] Au clusters can catalyze a range of reactions, for example, the water–gas shift reaction[12–14] and selective oxidation of carbon–carbon double bonds[15,16] and carbon–oxygen bonds.[17,18] The 4-nitrophenol

R. Cai, J. Liu, R. Griffin, Dr. W. Theis
Nanoscale Physics Research Laboratory
School of Physics and Astronomy
University of Birmingham
Birmingham B15 2TT, UK
R. Cai, Prof. R. E. Palmer
College of Engineering
Swansea University
Bay Campus, Fabian Way, Swansea SA1 8EN, UK
E-mail: r.e.palmer@swansea.ac.uk

DOI: 10.1002/smll.201703734
Dr. P. R. Ellis, C. M. Brown, Dr. P. T. Bishop
Johnson Matthey
Blount's Court, Sonning Common, Reading RG4 9NH, UK
Dr. J. Yin, Dr. K. Cooke
Teer Coatings Ltd.
Berry Hill Industrial Estate
Droitwich, Worcestershire WR9 9AS, UK
G. Chang, Prof. D. Yang
Collaborative Innovation Center for Marine Biomass Fibers Materials and Textiles of Shandong Province
School of Environmental Science and Engineering
Qingdao University
Qingdao 266071, P. R. China
Prof. J. Ren
School of Chemical and Environmental Engineering
North University of China
Taiyuan 030051, P. R. China

reduction by sodium borohydride ($NaBH_4$) is considered to be a standard model catalytic reaction[19,20] to evaluate nanocatalyst activity; precise optical measurement of the amount of 4-nitrophenol at very low concentrations is feasible. It is commonly believed that this reaction follows a Langmuir–Hinshelwood (LH) mechanism (**Figure 1**),[21,22] in which 4-nitrophenol is adsorbed on the surface of Au particles and reacts with activated hydrogen on the surface formed by decomposition of $NaBH_4$. It is thought that adding to Au a second metal element, M, which has a larger adsorption energy for nitrophenol than Au, can enhance the reaction rate.[23] The O—N bonds from the nitro group become weaker due to the electron delocalization from the O to the metal atoms, which directly correlates to the reaction rate. Based on this understanding, much effort has been made to produce Au/M bimetallic clusters on different supports and investigate their catalytic performance. For example, Pretzer et al.[24] synthesized Au nanoparticles decorated with palladium (Pd) and found that the activity of the Pd/Au catalyst is 5.5 (13) times that of pure Au (Pd) nanoparticles. Similar evidence of synergistic effects in nitrophenol and nitrothiophenol reduction over Au/Ni catalysts is reported.[25]

The use of copper (Cu) as an additive to improve the activity of noble metal clusters has become a "hot topic" because it can decrease the cost of catalysts and improve catalytic properties simultaneously.[26] It has been reported that adding Cu to Au nanoparticles can significantly improve their catalytic activity in many reactions, for example, CO oxidation.[27–30] However, for nitrophenol reduction catalyzed by Au/Cu bimetallic clusters, limited reports can be found and the catalytic mechanism is unconfirmed. It is commonly believed that Cu has a stronger interaction with the nitro group of nitrophenol than Au, which increases the adsorption energy of nitrophenol on the catalyst surface. Deposition of Au on the surface of Cu nanoparticles by a chemical method led to catalytic activity for 4-nitrophenol reduction that was enhanced by one order of magnitude in comparison with pure Au catalyst.[31] However, there was no clear evidence that the enhanced activity results from a synergetic effect between Au and Cu, since no Au/Cu alloy structure was observed. Au/Cu bimetallic clusters produced on planar sapphire substrates were active for 4-nitrophenol reduction and the activity could be enhanced by visible light (due to the localized surface plasmon resonance).[32] But the activity without excitation of the light was not explored. Thus, it is important to clarify the active sites in the Au/Cu system due to their significance in catalyst design. Traditionally, Au/Cu bimetallic clusters have been efficiently prepared by various chemical methods, for example, co-impregnation,[33] deposition-precipitation,[34] colloidal methods,[35] etc. However, a common disadvantage of these chemical methods is the presence of residual impurities, coming from the anion group of the metal salts not fully burned off in the calcination process or from capping ligands, as used purposely to reduce cluster aggregation. Some researchers report that capping ligands can either decrease the cluster activity by hindering reagent access to the catalyst[36,37] or can increase the activity via electron donation.[38] The existence of these impurities complicates the explanation of the original catalytic activity of the cluster, and can sometimes lead to misinterpretations. Moreover, another major challenge for chemical synthesis of binary nanoparticles is making sure that all the Au and Cu atoms are alloyed inside the clusters. A well-controlled way to make naked Au/Cu nanoparticle catalysts is desirable.

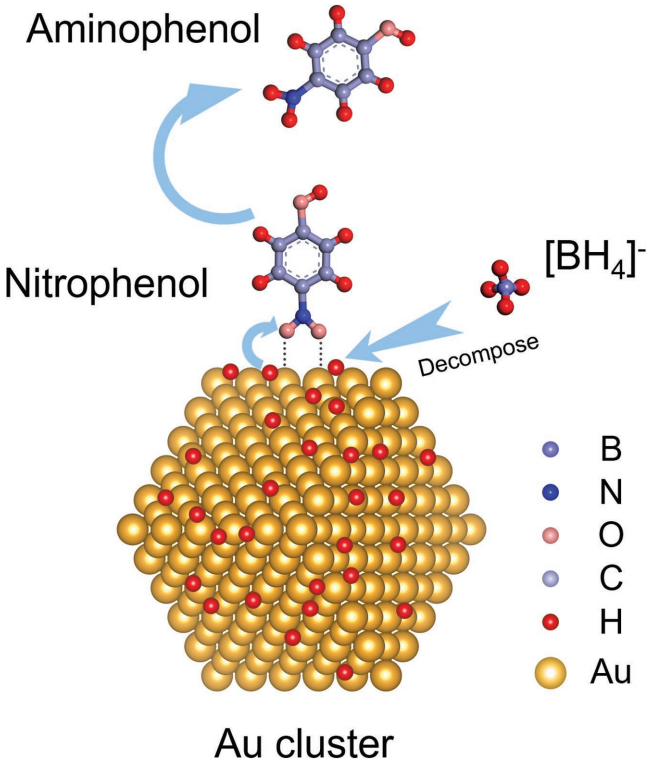

Figure 1. Schematic diagram of catalytic reduction of 4-nitrophenol on an Au cluster by $NaBH_4$, following a Langmuir–Hinshelwood mechanism.

In this work, we employed a dual-magnetron sputtering gas condensation cluster source to produce Au/Cu bimetallic clusters deposited onto an inert powder support, magnesium oxide (MgO). By changing the power applied to the two targets (Au, Cu), the average Au/Cu ratio can be tuned. Aberration-corrected scanning transmission electron microscopy (STEM) in high-angle annular dark-field (HAADF) mode, coupled with energy-dispersive X-ray spectroscopy (EDS), reveals that the Au/Cu bimetallic clusters formed have a random alloy structure. We find that these bimetallic clusters are much more active in selective nitrophenol hydrogenation than pure Au or Cu clusters, and 25 times for active than reference Au/Cu binary nanoparticles produced by impregnation. The interplay between surface Au and Cu sites is deduced to create the most active site for reaction. Our study thus validates the performance of the new nanoalloy materials in a solution phase reaction, and provides an insight into nanocatalyst design of bimetallic systems at the atomic scale.

2. Results and Discussion

2.1. Analysis of Magnetron Sputtering Deposited Au/Cu Bimetallic Clusters

Au/Cu clusters with three different Au/Cu ratios—that we term Au-rich, Au/Cu-equal (approximately), and Cu-rich—were

produced by applying sputtering powers to the Au and Cu targets of 6 W:3 W, 6 W:6 W, and 3 W:6 W, respectively. The cluster size was characterized by two methods, time-of-flight mass filtering which gives cluster size (mass) information before depositing onto the supports, and STEM which provides cluster size (diameter) information after landing on the supports. **Figure 2** shows mass spectra obtained during the deposition as well as STEM cluster diameter distribution histograms for the following samples: (a), (d) Au-rich; (b), (e) Au/Cu-equal; and (c), (f) Cu-rich. The insets show typical low-magnification HAADF images of the kind used to acquire the cluster diameter histograms. From the mass spectra, the Au-rich and Cu-rich clusters have peaks at similar masses of ≈40 000 amu, which is equivalent to the size of Au_{200}, whereas the Au/Cu-equal clusters peak at a larger value of ≈65 000 amu, equivalent to the size of Au_{300}. The cluster diameter histograms based on the HAADF images also show the same trend, that is, that Au-rich clusters and Cu-rich clusters have a smaller cluster diameter ≈3.6 nm, than Au/Cu-equal clusters, ≈4.6 nm. To clarify if agglomeration takes place after clusters land on the support, the diameter of the Au/Cu-equal clusters at the peak position in the mass spectrum is estimated based on the cluster volume assuming a quasi-spherical shape. If the cluster composition is assumed to be Au_1Cu_1 and the cluster has a spherical shape on the support, the diameter of a cluster with a mass of 65 000 amu should be ≈2.4 nm (≈3.0 nm for hemispherical clusters), which is much smaller than the average diameter, 4.6 nm, obtained from HAADF images. This indicates that the Au/Cu-equal clusters are larger because they aggregate on the support surface, or possibly lose their spherical shape after landing on the support. In the HAADF images, some large clusters formed by coalescence can easily be observed. It should be noted that the surface agglomeration which happens during the deposition process occurs because the powder supports in the vibration cup cannot be agitated entirely evenly, especially when they are charged by the cluster ion beam, leading to uneven cluster coverage. This behavior occurs for all three samples. Such surface agglomeration has also been reported for deposition of Fe—Co nanoalloy clusters onto carbon supports by dual plasma guns.[39]

Table 1 shows the inductively coupled plasma (ICP) results as a function of sputtering power applied to each target, yielding the Au-rich, Au/Cu-equal (approximately), and Cu-rich nanoalloy samples. It can be seen from the table that the total metal loadings of these three samples are different, but the atomic ratios of Au and Cu in Au-rich, Au/Cu-equal, and Cu-rich samples are 3.87:1, 1.16:1, and 0.45:1, respectively, which indicates the overall catalyst composition is strongly dependent on the power applied to each target. To identify the distributions of Au and Cu atoms inside the clusters, compositional line profiles across individual clusters in each kind of sample were obtained by EDS line scanning (**Figure 3**). Within the clusters, both Au and Cu signals are detected in each of these three samples and no obvious valleys or peaks are observed, which suggests Au atoms and Cu atoms are mixed together instead of forming core–shell or Janus structures. Theoretically, mixing of Au and Cu is energetically favored in Au/Cu compounds compared with separated phases.[40–43] In addition, a steady increase of Cu signal observed from the Au-rich sample to the Cu-rich sample confirms the increasing Cu content inside the clusters.

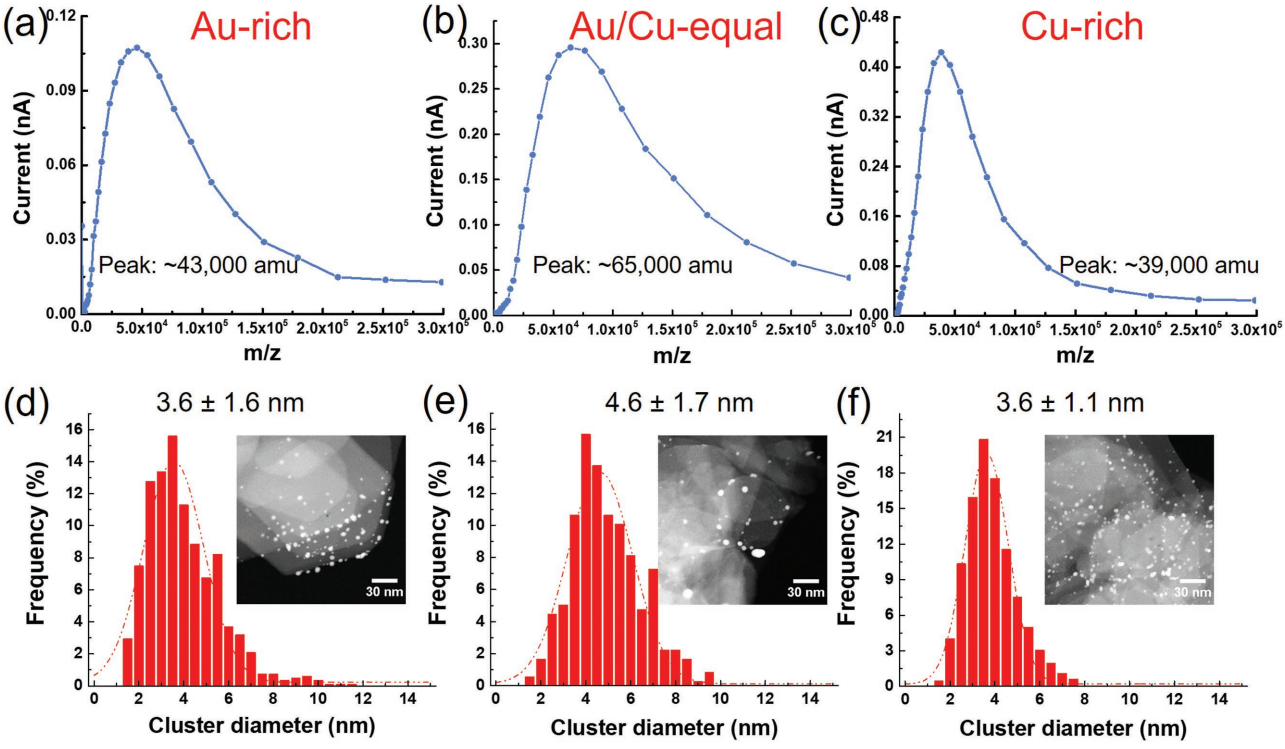

Figure 2. a–c) Mass spectra obtained during the cluster deposition process, and d–f) diameter distributions of Au/Cu bimetallic clusters on MgO powder with different Au/Cu ratios; a,d) Au-rich, b,e) Au/Cu-equal, c,f) Cu-rich. The insets are the corresponding low-magnification HAADF images.

Table 1. ICP results of the Au/Cu nanoalloy clusters produced as a function of the power applied to the Au and Cu targets.

Sample	Au/Cu target power	Au loading wt%	Cu loading wt%	Au/Cu atomic ratio
Au-rich	6 W:3 W	0.12	0.01	3.87: 1
Au/Cu-equal	6 W:6 W	0.18	0.05	1.16: 1
Cu-rich	3 W:6 W	0.07	0.05	0.45: 1

To investigate the atomic structure of the Au/Cu bimetallic clusters, high-resolution HAADF images were acquired as shown in **Figure 4**. Figure 4a shows the typical HAADF image of an Au-rich cluster with a crystal domain aligned along the [111] zone-axis. The crystal planes marked by red lines correspond to $(2\bar{2}0)$ planes with an interplanar spacing of 1.39 Å, which lies between the interplanar spacing of $(2\bar{2}0)$ planes for pure Au (1.44 Å) and pure Cu (1.28 Å). The same trend is also found in an Au/Cu-equal cluster (Figure 4b) and a Cu-rich cluster (Figure 4c); again the measured interplanar spacings of the (002) planes are between those of pure Au and pure Cu. This result further supports the Au/Cu alloy structure, according to Vegard's law.[44] In addition, Yin et al. distinguished the Au/Cu core/shell structure through observing the intensity contrast of HAADF STEM images.[45] A trough or a peak was observed in the intensity line profile across an Au/Cu cluster with core/shell structure. For our Au/Cu bimetallic clusters, it is apparent

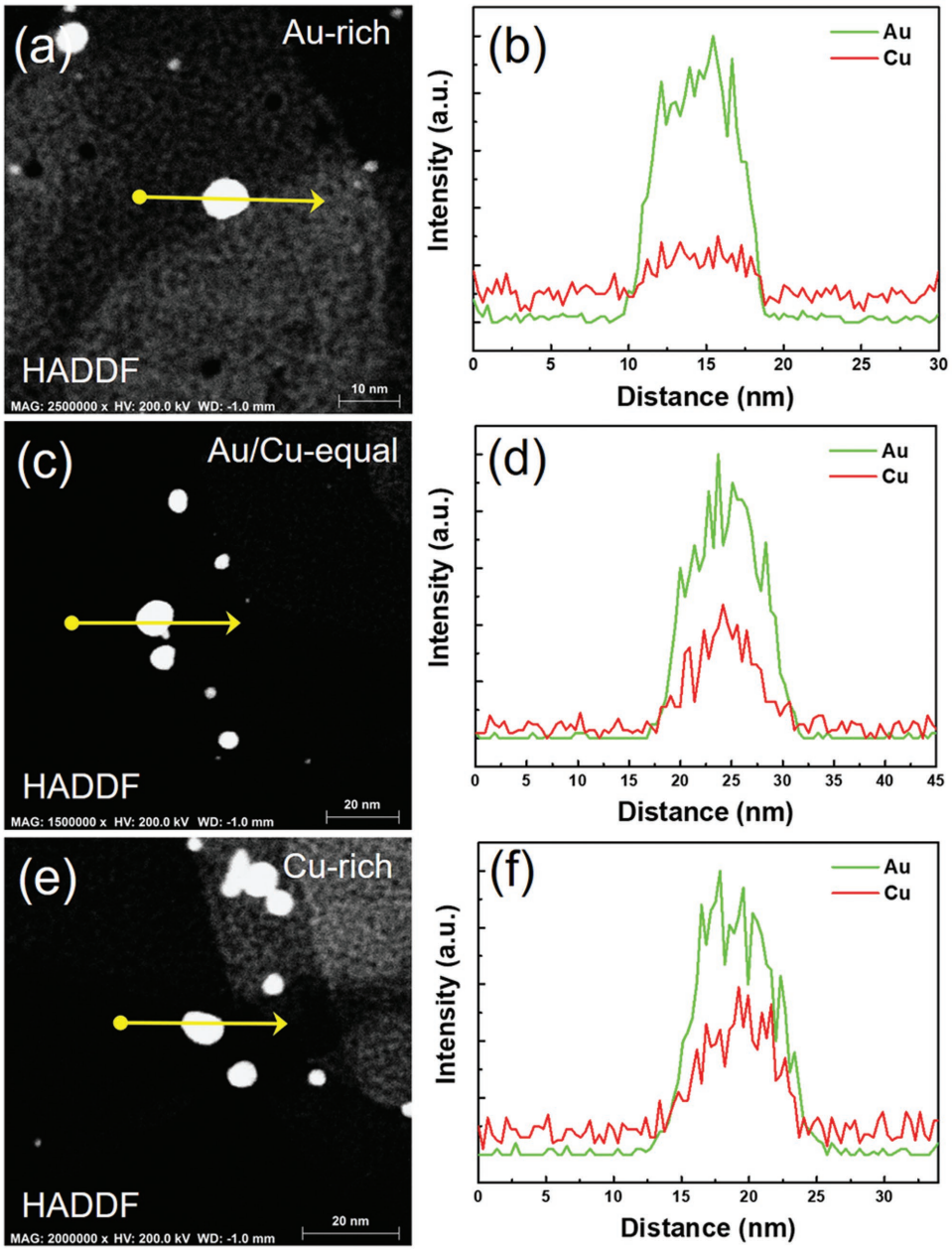

Figure 3. Typical HAADF images and corresponding EDS line scanning results for a,b) Au-rich clusters, c,d) Au/Cu-equal clusters, and e,f) Cu-rich clusters.

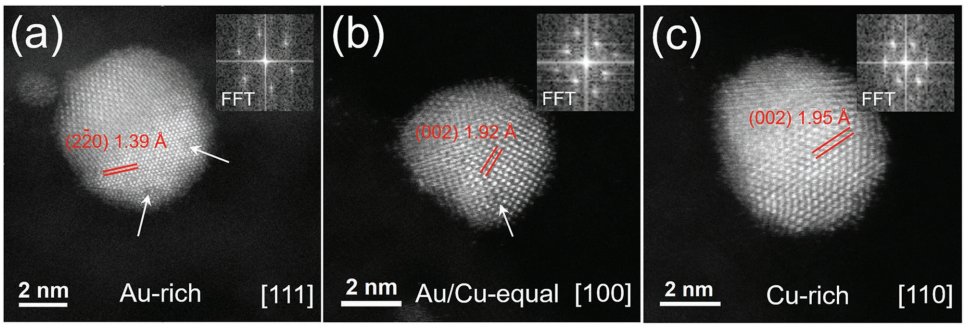

Figure 4. Typical high-resolution HAADF images of a) an Au-rich cluster with a crystal domain aligned along the [111] zone-axis, b) an Au/Cu-equal cluster with a crystal domain aligned along the [100] zone-axis, and c) a Cu-rich cluster with a crystal domain aligned along the [110] zone-axis. The insets are the FFT images corresponding to the crystal domains in each cluster.

that no clear core–shell structure exists, which is consistent with the EDS line scanning results. This alloy structure is also observed in clusters of other orientations and amorphous clusters from all the three samples by distinguishing the HAADF intensity of STEM images. The alloy structure we find has also been reported in chemically prepared Au/Cu bimetallic clusters by other groups.[46] For the bulk Au/Cu alloy, chemically ordered structures are energetically favored and chemically ordered Au_3Cu, Au_1Cu_1, and Au_1Cu_3 phases are found at low temperature. Here, Cu atoms and Au atoms are arranged periodically. In electron diffraction patterns, chemically ordered structures can lead to the appearance of superstructure diffraction spots along certain directions.[47,48] For example, in Au_1Cu_3 nanorods, a [110] oriented chemical ordering was observed by monitoring the appearance of (110) superstructure diffraction spots in the electron diffraction pattern.[49] To confirm the absence of chemical ordered structures in our Au/Cu bimetallic clusters, fast Fourier transforms (FFT) have been calculated for the STEM image of clusters shown in Figure 4 and are displayed as inset. If the ordered structures—Au_3Cu_1, Au_1Cu_1, or Au_1Cu_3—exist in the clusters, the superstructure diffraction spots from (110) or (100) planes should appear in the FFT images. However, in the insets to Figure 4, no superstructure diffraction spots are observed at all, which indicates that Au and Cu atoms are randomly located in the clusters and there is no chemical ordering. Finally, the intensity of columns in the HAADF images is related to the Z number of atoms.[50] The heavier the atom, the higher the intensity.[51] Considering Cu is much lighter than Au, it is reasonable to assume that lower column intensity corresponds to more Cu atoms in a column. In Figure 4a,b, some atom columns are significantly darker than the adjacent columns, highlighted by white arrows, which suggests that more Cu atoms are located in these darker columns than in the neighbors. Again, this behavior is consistent with a random alloy structure.

2.2. Evaluation of Catalytic Activity for 4-Nitrophenol Reduction by $NaBH_4$

After adding $NaBH_4$ to the nitrophenol solution, 4-nitrophenolate ions are formed, which show a strong visible absorbance at 400 nm.[52] The intensity of the absorbance peak, proportional to the concentration of 4-nitrophenolate ions, is used to evaluate the progress of the reaction. **Figure 5** shows typical UV–vis absorbance spectra with time intervals of 5 min after adding of Au-rich, Au/Cu-equal, and Cu-rich cluster catalysts supported on MgO. It is obvious that in the case of the Au/Cu-equal cluster catalyst, on adding the catalyst into the reaction mixture, the absorbance peak at 400 nm decreases immediately and continuously. However, in the case of the Au-rich and Cu-rich cluster catalysts, the peak intensity decreases much more slowly, which indicates that these catalysts are less active than the Au/Cu-equal catalysts.

The reduction of 4-nitrophenol catalyzed by metal particles is considered pseudo-first order with respect to the concentration of

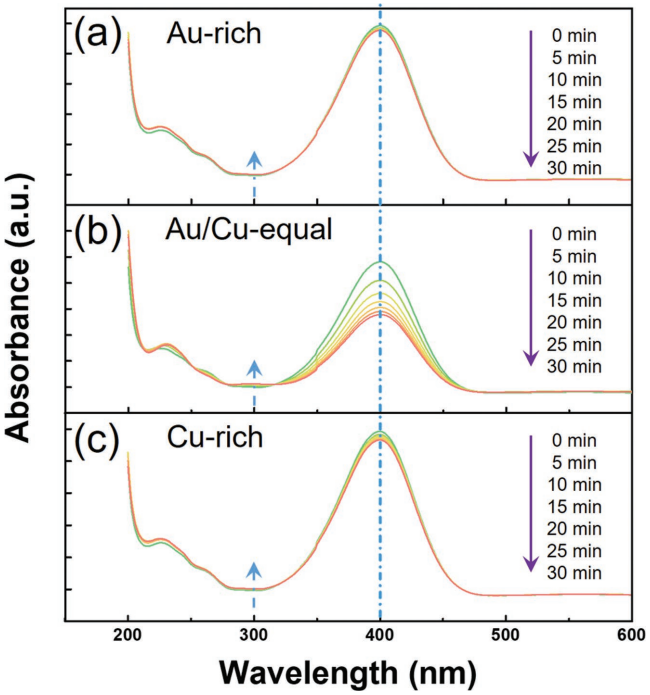

Figure 5. UV–vis absorbance spectra during the 4-nitrophenol reduction by $NaBH_4$ (5 min intervals), in presence of Au/Cu bimetallic cluster catalysts on MgO support with different Au/Cu ratios, a) Au-rich, b) Au/Cu-equal, and c) Cu-rich. The absorbance peak at 400 nm corresponds to 4-nitrophenol and the peak intensity relates to the concentration.

4-nitrophenol in the presence of a large excess of $NaBH_4$.[53,54] The apparent reaction rate constant k_{app}, which can be used to compare the activity of the catalysts, is defined through Equation (1)

$$\frac{dC_t}{dt} = -k_{app}C_t \quad (1)$$

Here, C_t represents the concentration of nitrophenol at time t. Because the optical absorbance at time t (A_t) is proportional to C_t, a plot of C_t/C_0 and thus $-\ln(C_t/C_0)$ versus t can be acquired easily from the absorbance, as shown in **Figure 6**. C_0 is the initial concentration of 4-nitrophenol. In accordance with the pseudo-first-order kinetic assumption, the relationships for C_t/C_0 and $-\ln(C_t/C_0)$ versus reaction time are fitted by an exponential decay and linear growth, respectively. The apparent reaction rate constant is obtained from the linear slope in Figure 6. The k_{app}

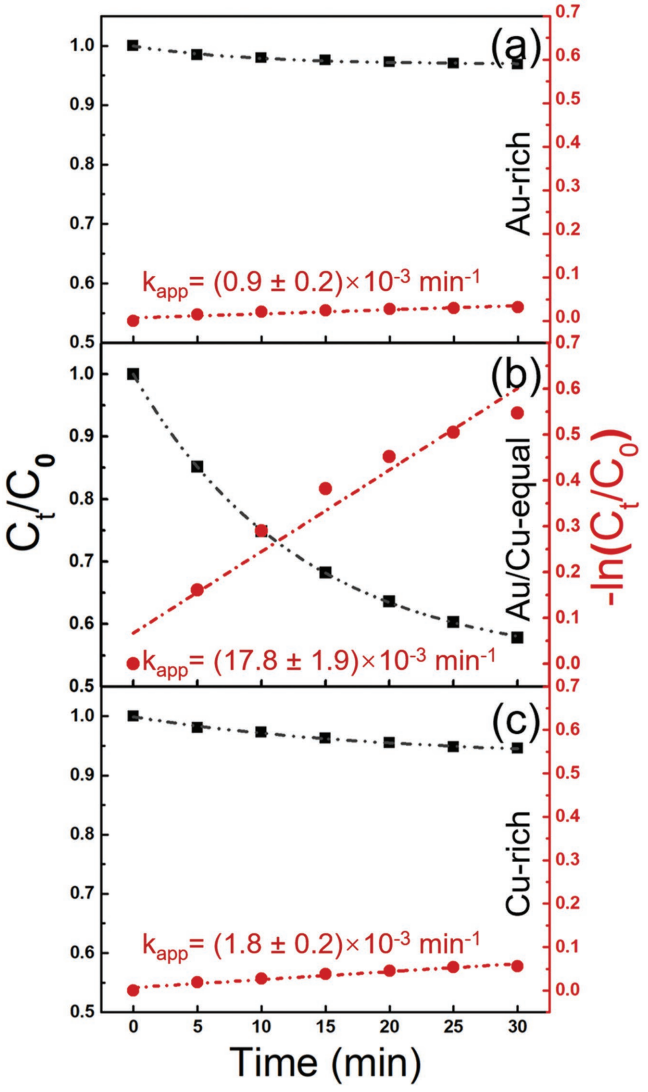

Figure 6. Plots of nitrophenol concentration, C_t/C_0 and $-\ln(C_t/C_0)$, versus time for the nitrophenol reduction by $NaBH_4$ over a) Au-rich, b) Au/Cu-equal, and c) Cu-rich cluster catalysts on MgO. The slope of the red fitting lines shows the apparent reaction rate constant.

Table 2. Comparison of the apparent reaction rate constant k_{app} and the intrinsic reaction rate constant k_{nor} normalized by the total number of moles of metal for the reduction of nitrophenol catalyzed by Au/Cu cluster catalysts.

Sample	k_{app} [×10^{-3} min^{-1}]	k_{nor} [×10^4 min^{-1} mole of metal^{-1}]
Au-rich	0.9 ± 0.2	0.39 ± 0.09
Au/Cu-equal	17.8 ± 1.9	3.49 ± 0.37
Cu-rich	1.8 ± 0.2	0.53 ± 0.06
Au/Cu reference	1.7 ± 0.1	0.14 ± 0.01

obtained for the Au/Cu-equal cluster catalyzed reaction is 17.8 × 10^{-3} min^{-1}, which is almost 20 (10) times higher than that obtained for the Au-rich (Cu-rich) clusters. Considering the difference of metal loading in these three samples, the intrinsic reaction rate constant k_{nor} is calculated by normalizing the k_{app} values by the number of moles of metal as summarized in **Table 2**. The normalized reaction rate constant k_{nor} for Au/Cu-equal clusters is 3.49 × 10^4 min^{-1} mol^{-1}, which is 8.9 (6.6) times that of Au-rich (Cu-rich) clusters. It should also be noted that, compared with the Au-rich catalyst, the Cu-rich catalyst has a lower metal loading but higher normalized activity, indicating the Cu-rich clusters are more active than Au-rich clusters. We will discuss this behavior below.

In addition, we also compared the catalytic activity of the Au/Cu-equal cluster on MgO sample with the reference catalyst (Au_1Cu_1 on MgO powder) produced by the traditional impregnation method. The k_{nor} for the reference sample is 0.14 × 10^4 min^{-1} mole of metal^{-1}, which is 25 times smaller than that for the Au/Cu-equal cluster sample (see Table 2 and Figure S2a, Supporting Information). A list of recent studies on the 4-nitrophenol reduction over chemically produced Au and Cu based catalysts is summarized in Table S2 (Supporting Information) together with our Au/Cu-equal cluster catalyst. Although the intrinsic reaction rate constant obtained for the new cluster catalyst is not yet competitive with the best Au catalysts synthesized chemically, this method still provides a way to establish the original catalytic activity of "naked" clusters.

2.3. Discussion of the Catalytic Activity for 4-Nitrophenol Reduction over Au/Cu Nanoalloy Cluster Catalysts and Model Calculations

The principal topics for discussion arising from the experimental results concern: (i) why the random nanoalloy Au/Cu-equal cluster catalysts supported on MgO are so much more active than the Au-rich or Cu-rich clusters and (ii) why the Au/Cu-equal cluster catalysts are significantly more active than the reference Au/Cu catalysts generated by impregnation. In addressing these questions, we also bear in mind the results that Cu-rich clusters are somewhat more active than Au-rich clusters. A central issue in understanding the enhancement of catalytic activity must be the nature of the binding of the principal reactant (4-nitrophenol) and product (4-aminophenol) to the MgO-supported Au/Cu nanoparticles.

To shed some light on the interaction between the reactant (product) and the clusters we have conducted illustrative

calculations of the binding of 4-nitrophenol (4-aminophenol) to model Au_{13}, Cu_{13}, and $Au_{12}Cu_1$ free clusters. Details of the calculations are given in the Supporting Information. Of course these model clusters are much smaller than those employed in the experiments; nevertheless, they are sufficient to investigate the effects of local bonding to Au, Cu, and Au/Cu sites at the surface of our 3–5 nm clusters. **Figure 7** shows the density functional theory (DFT) optimized model of 4-nitrophenol and 4-aminophenol on Au_{13}, Cu_{13}, and $Au_{12}Cu_1$ clusters. The nitrophenol bonds with two metal atoms through the two O atoms from the nitro group. As expected, the two metal–O bonds from the nitro group are much longer on the Au cluster (3.18 and 3.29 Å) than on the Cu cluster (2.34 and 1.95 Å), which reflects the fact that nitrophenol has a much stronger interaction with Cu than Au. Whereas for the $Au_{12}Cu_1$ clusters, the nitro group is bonded on an Au/Cu site and the lengths of the two metal–O bonds, Au—O bond (3.13 Å) and Cu—O bond (2.20 Å), are similar to those of the Au—O bond on the Au cluster and Cu—O bond on the Cu cluster, respectively. This indicates that the substitution of Cu in the Au cluster is helpful for 4-nitrophenol adsorption. The calculated adsorption energies of 4-nitrophenol on model clusters further confirm this conclusion. For

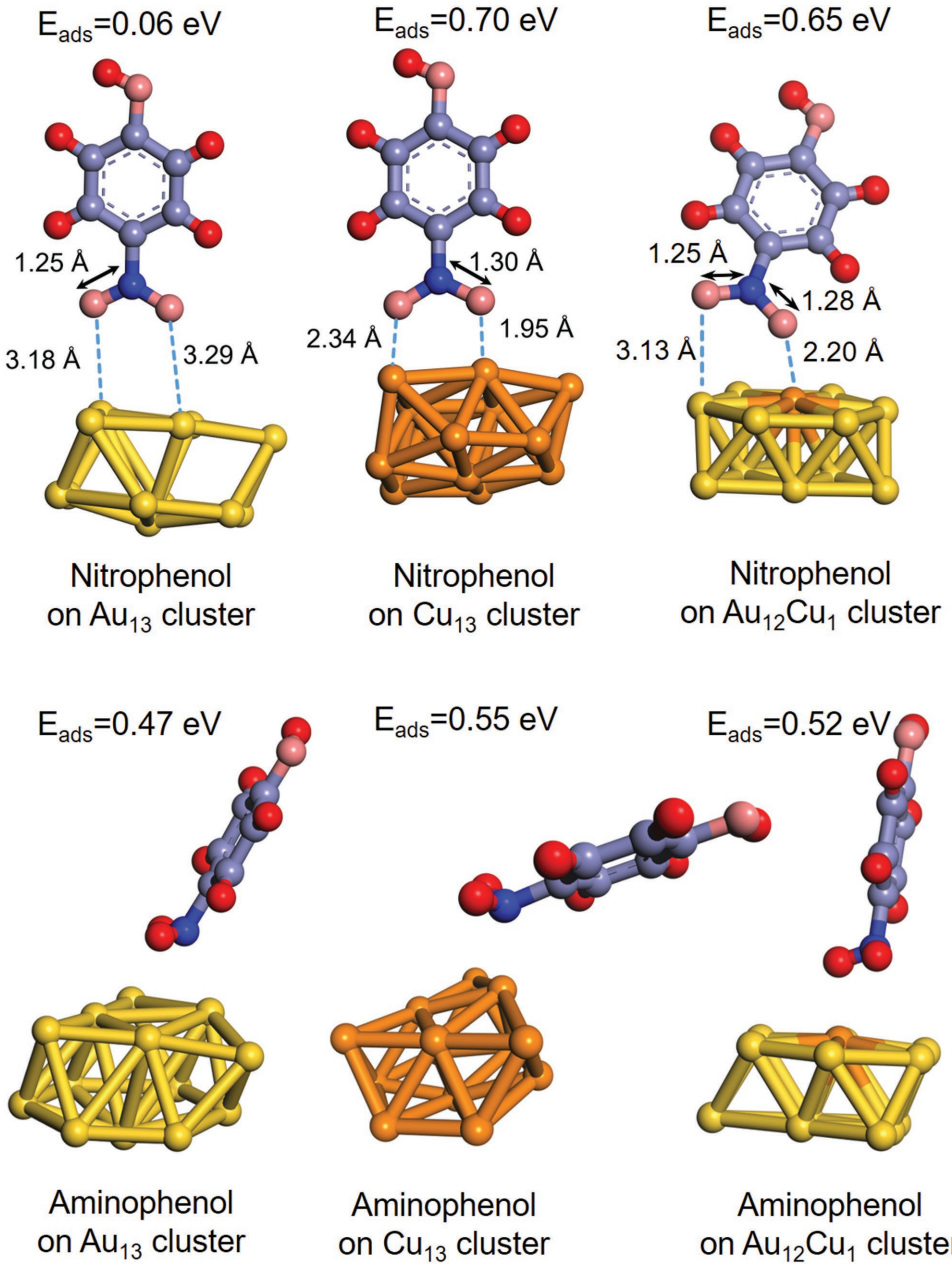

Figure 7. DFT-simulated 4-nitrophenol and 4-aminophenol on Au_{13}, Cu_{13}, and $Au_{12}Cu_1$ clusters. The substitution of the Cu atom in the Au cluster optimized the adsorption of 4-nitrophenol and desorption of 4-aminophenol, which enhanced the catalytic activity for the whole reaction. (Atom colors as in Figure 1.)

the $Au_{12}Cu_1$ cluster the bonding energy with the nitrophenol molecule is 0.65 eV compared with 0.06 eV for the Au cluster and 0.70 eV for the Cu cluster. In addition, due to the electron delocalization from O to the metal, on the $Au_{12}Cu_1$ cluster the length of the O—N bond on Cu atom (1.28 Å) is longer than that on Au atom (1.25 Å), so the N—O bond on Cu atom is much easier to cleave. However, the catalyst activity is also affected by the desorption of the product. The calculated adsorption energy of 4-aminophenol on $Au_{12}Cu_1$ clusters (0.52 eV) is larger than that on the Au cluster (0.47 eV), but smaller than that on Cu clusters (0.55 eV), manifesting the aminophenol molecule also has a stronger interaction with Cu than Au. Thus, although Cu is beneficial for the adsorption of the nitrophenol and for cleavage of the N—O bonds, it also hinders the release of the product, which results in a limited catalytic activity.

The results from the model calculations, namely, that Cu has a stronger interaction than Au with both the reagent, 4-nitrophenol, and the product, 4-aminophenol, provide an appealing basis for explaining why the Au/Cu-equal clusters are the most active for the reduction of the nitrophenol. Assuming the reaction follows an LH mechanism, the reduction takes place on the cluster surface. For the pure Au cluster, the catalytic activity is limited by the weak adsorption of nitrophenol, whereas the pure Cu cluster has an overly strong interaction with the aminophenol, which hinders the desorption of the product and again leads to limited activity. The combination of Au with Cu increases the adsorption energy of the nitrophenol compared with gold and reduces the adsorption energy of aminophenol compared with copper. We have shown that the optimized adsorption configuration for this reaction involves the nitro group bonding with adjacent Au and Cu sites through the two O atoms; then the abundance of Au/Cu sites on the cluster surface will regulate the catalytic activity. Given the random arrangement of Au and Cu atoms inside the clusters, more Au/Cu sites exist on the Au/Cu-equal cluster surface than Au-rich and Cu-rich clusters, which gives a reason why the Au/Cu-equal cluster catalyst exhibits the highest catalytic activity. Moreover, we can associate the higher catalytic activity of the Cu-rich clusters than the Au-rich clusters with the fact that the Au/Cu atomic ratio obtained is closer to 1:1 in the Cu-rich clusters (0.45:1) compared with the Au-rich clusters (3.87:1), which allows for more of the proposed Au-Cu active sites on the surface of the Cu-rich clusters.

The reason why the Au/Cu-equal cluster catalyst is much more active than the Au/Cu reference sample may be associated with the diameter distribution and composition of the clusters in the reference sample, see Figure S2b and Table S1 (Supporting Information). Compared with the Au/Cu-equal catalyst, the clusters in the Au/Cu reference sample have much larger diameter (≈10 nm), which is traceable to the calcination process at high temperature. Due to the lower specific surface area for the larger clusters, the reference sample presents significantly fewer Au/Cu active sites on the surface per unit mole of catalyst. In addition, the ICP results show that the Au/Cu atomic ratio for the reference sample is 0.69:1 after the calcination, which should decrease the number of the Au/Cu sites on the cluster surface. So the unbalanced composition achieved in our impregnation method after calcination may combine with the larger size to give the reduced activity for the reference sample compared with the Au/Cu-equal clusters. The result emphasizes the utility of the cluster beam method in generating nanoparticle catalysts of tunable size below 10 nm and well-defined composition.

3. Conclusion

The performance of Au/Cu bimetallic nanoparticles in a model solution phase catalytic reaction has been validated. The nanoalloy clusters were produced by a dual-target magnetron sputtering and gas condensation cluster source and deposited onto MgO powder supports in vacuum. The composition of the Au/Cu catalysts can be controlled by tuning the power applied to the sputtering targets. EDS line scanning spectra and Z-contrast STEM images reveal that the Au/Cu bimetallic clusters, whether Au-rich, Cu-rich, or Au/Cu-equal, have a random alloy structure without chemical ordering. The catalytic performance of the three types of MgO-supported catalysts in the reduction of 4-nitrophenol by $NaBH_4$ has been investigated by UV–vis spectrophotometry. A normalized intrinsic reaction rate constant of 3.49×10^4 min^{-1} mole of $metal^{-1}$ is obtained from the Au/Cu-equal cluster catalyst, which is 8.9 (6.6) times higher than the Au-rich (Cu-rich) clusters. The enhanced catalytic activity of the Au/Cu-equal catalyst is deduced to result from a higher abundance of Au/Cu sites on the surface of the Au/Cu-equal clusters compared with the other two samples. Model theoretical calculations of Au, Cu, and Au/Cu clusters show that the proximity of Au and Cu surface sites enables a balancing of the adsorption of 4-nitrophenol and desorption of 4-animophenol, which increases the catalytic activity for the system. Moreover, we have demonstrated that physically deposited Au/Cu-equal catalysts show an activity 25 times higher than an Au/Cu reference sample made by the chemical impregnation method. The results validate the performance of this new class of nanoalloy catalysts generated by cluster beam deposition in an important model selective transformation in the liquid phase.

4. Experimental Section

Au/Cu Cluster Deposition: The clusters were produced in a dual-target magnetron sputtering gas condensation cluster source (at Teer Coatings). Au/Cu clusters with three different Au/Cu ratios were deposited on agitated MgO powder supports. A schematic diagram of the system is shown in Figure S1 (Supporting Information). Detailed information can be found in an earlier report.[5] In the magnetron sputtering chamber, two magnetrons (copper and gold) are mounted in parallel with a condensation length (the distance between these targets and the exit nozzle of the condensation chamber) of 24 cm. The sputtering power applied to each magnetron was separately controlled in order to tune the material ratio in the resulting binary clusters. Au and Cu atoms were sputtered out from the targets and condensed in cold Ar/He gas to form Au/Cu clusters of various sizes. A pressure of ≈0.21 mbar was maintained in the condensation chamber, with 100 standard cubic centimeters per minute (sccm) Ar flow and 20 sccm He flow. Positively charged clusters were extracted, accelerated, and guided by a series of ion optical lenses. The ultimate flight direction of the cluster beam was controlled by an "octosphere" deflector that can transmit the cluster beam forward into a lateral time-of-flight mass filter[55] to measure the clusters' size distribution or bend the beam through 90° to propagate vertically toward a lower chamber for powder deposition. In this

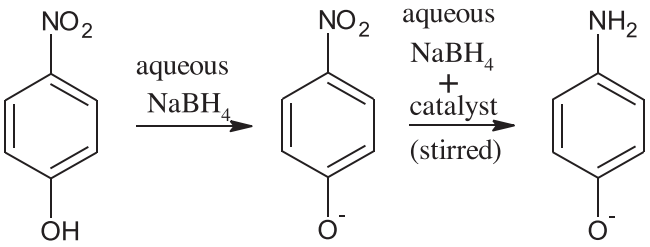

Scheme 1. Reaction scheme of 4-nitrophenol reduction by $NaBH_4$.

deposition chamber, the powder supports (0.8 g MgO powders) were loaded into a cup which is agitated continuously to maximize exposure of all the powder to the cluster beam. In addition, during the deposition process, the cup was biased with a potential of –1 kV to accelerate and thus help immobilize clusters on the powder surface.

The Au/Cu reference sample was made by a traditional impregnation method[27] on the same support. Detailed information can be found in the Supporting Information. The support used in this experiment was MgO powder obtained from Alfa Aesar with particle size between 100 and 200 nm. The powder itself was tested and confirmed to be catalytically inert for the nitrophenol reduction reaction.

Characterization of Au/Cu Nanoalloy Clusters on MgO Powder Supports: The elemental composition of the cluster catalysts was characterized by EDS in the STEM and inductively coupled plasma mass spectrometry following digestion in aqua regia. The cluster size and atomic structure were characterized by a JEOL JEM-2100F scanning transmission electron microscope equipped with a C_s probe corrector (CEOS) at a convergence angle of 20 mrad and a HAADF detector operating with inner angle of 62 mrad and outer angle of 164 mrad at 200 kV. STEM samples were prepared by dispersing the MgO powder decorated with clusters in deionized water, sonicating for several minutes and drop-casting onto a nickel grid coated with an amorphous carbon film.

4-Nitrophenol Reduction Measurement: The reduction of 4-nitrophenol was carried out in aqueous solution at room temperature with $NaBH_4$ acting as the reductant. The reaction scheme is shown in **Scheme 1**. 4-Nitrophenol (1.67 mg, Sigma-Aldrich) and $NaBH_4$ (18.92 mg, Sigma-Aldrich) were added in deionized water (200 mL) sequentially, which gave a 4-nitrophenol concentration of 0.06×10^{-3} M and $NaBH_4$ concentration of 2.5×10^{-3} M. After shaking the solution for 2 min, the color became yellow, which indicated 4-nitrophenol conversion to 4-nitrophenolate.[56] For each test, 30 mg catalyst was added to 50 mL of this solution and continuously magnetically stirred. To monitor the reaction process, the optical absorbance of the reaction solution was recorded by a UV–vis spectrophotometer (Agilent Technologies Cary Series) at intervals of 5 min. For each measurement, 2 mL of the analyte solution was filtered by a syringe filter (pore size: 0.2 µm) to remove the catalyst and poured into a cuvette.

Supporting Information

Supporting Information is available from the Wiley Online Library or from the author.

Acknowledgements

This research was funded by the EPSRC (Grant Reference No. EP/K006061/1) and by the European Union's Seventh Framework Programme (No. FP7/2007-2013) under Grant Agreement No. 607417 (CATSENSE). The authors would like to thank Mr. Matthew Rose, Mr. Ian Briggs, and Mr. Paul Fisher at Johnson Matthey for the ICP measurement.

Conflict of Interest

The authors declare no conflict of interest.

Keywords

Au/Cu nanoparticles, catalysis, cluster beam deposition, nanoalloys, nitrophenol reduction

Received: October 26, 2017
Revised: December 26, 2017
Published online: February 7, 2018

[1] R. E. Palmer, S. Pratontep, H.-G. Boyen, *Nat. Mater.* **2003**, *2*, 443.
[2] E. T. Baxter, M.-A. Ha, A. C. Cass, A. N. Alexandrova, S. L. Anderson, *ACS Catal.* **2017**, *7*, 3322.
[3] C. Liu, B. Yang, E. Tyo, S. Seifert, J. DeBartolo, B. von Issendorff, P. Zapol, S. Vajda, L. A. Curtiss, *J. Am. Chem. Soc.* **2015**, *137*, 8676.
[4] M. Rondelli, G. Zwaschka, M. Krause, M. D. Rtzer, M. N. Hedhili, M. P. Hgerl, V. D'Elia, F. F. Schweinberger, J.-M. Basset, U. Heiz, *ACS Catal.* **2017**, *7*, 4152.
[5] P. R. Ellis, C. M. Brown, P. T. Bishop, J. Yin, K. Cooke, W. D. Terry, J. Liu, F. Yin, R. E. Palmer, *Faraday Discuss.* **2016**, *188*, 39.
[6] S. Vajda, M. G. White, *ACS Catal.* **2015**, *5*, 7152.
[7] V. Habibpour, C. Yin, G. Kwon, S. Vajda, R. E. Palmer, *J. Exp. Nanosci.* **2013**, *8*, 993.
[8] M.-A. Ha, E. T. Baxter, A. C. Cass, S. L. Anderson, A. N. Alexandrova, *J. Am. Chem. Soc.* **2017**, *139*, 11568.
[9] E. C. Tyo, S. Vajda, *Nat. Nanotechnol.* **2015**, *10*, 577.
[10] M. Haruta, T. Kobayashi, H. Sano, N. Yamada, *Chem. Lett.* **1987**, *16*, 405.
[11] K.-J. Hu, S. R. Plant, P. R. Ellis, C. M. Brown, P. T. Bishop, R. E. Palmer, *J. Am. Chem. Soc.* **2015**, *137*, 15161.
[12] T. Magadzu, J. H. Yang, J. D. Henao, M. C. Kung, H. H. Kung, M. S. Scurrell, *J. Phys. Chem. C* **2017**, *121*, 8812.
[13] H. Xu, Y. Li, X. Luo, Z. Xu, J. Ge, *Chem. Commun.* **2017**, *53*, 7953.
[14] S. Yao, X. Zhang, W. Zhou, R. Gao, W. Xu, Y. Ye, L. Lin, X. Wen, P. Liu, B. Chen, E. Crumlin, J. Guo, Z. Zuo, W. Li, J. Xie, L. Lu, C. J. Kiely, L. Gu, C. Shi, J. A. Rodriguez, D. Ma, *Science* **2017**, *357*, 389.
[15] S. Karakalos, Y. Xu, F. C. Kabeer, W. Chen, J. C. F. Rodríguez-Reyes, A. Tkatchenko, E. Kaxiras, R. J. Madix, C. M. Friend, *J. Am. Chem. Soc.* **2016**, *138*, 15243.
[16] D. Ravelli, S. Protti, M. Fagnoni, *Chem. Rev.* **2016**, *116*, 9850.
[17] L. Wang, J. Zhang, G. Wang, W. Zhang, C. Wang, C. Bian, F.-S. Xiao, *Chem. Commun.* **2017**, *53*, 2681.
[18] D.-Y. Li, Y. Wei, M. Shi, *Adv. Synth. Catal.* **2016**, *358*, 3002.
[19] H. Ye, Q. Wang, M. Catalano, N. Lu, J. Vermeylen, M. J. Kim, Y. Liu, Y. Sun, X. Xia, *Nano Lett.* **2016**, *16*, 2812.
[20] N. Bingwa, R. Patala, J.-H. Noh, M. J. Ndolomingo, S. Tetyana, S. Bewana, R. Meijboom, *Langmuir* **2017**, *33*, 7086.
[21] P. Zhao, X. Feng, D. Huang, G. Yang, D. Astruc, *Coord. Chem. Rev.* **2015**, *287*, 114.
[22] R. Ciganda, N. Li, C. Deraedt, S. Gatard, P. Zhao, L. Salmon, R. Hernández, J. Ruiz, D. Astruc, *Chem. Commun.* **2014**, *50*, 10126.
[23] Z. D. Pozun, S. E. Rodenbusch, E. Keller, K. Tran, W. Tang, K. J. Stevenson, G. Henkelman, *J. Phys. Chem. C* **2013**, *117*, 7598.
[24] L. A. Pretzer, K. N. Heck, S. S. Kim, Y.-L. Fang, Z. Zhao, N. Guo, T. Wu, J. T. Miller, M. S. Wong, *Catal. Today* **2016**, *264*, 31.
[25] A. B. Vysakh, C. L. Babu, C. P. Vinod, *J. Phys. Chem. C* **2015**, *119*, 8138.
[26] A. S. Bandarenka, A. S. Varela, M. Karamad, F. Calle-Vallejo, L. Bech, F. J. Perez-Alonso, J. Rossmeisl, I. E. L. Stephens, I. Chorkendorff, *Angew. Chem., Int. Ed.* **2012**, *51*, 11845.
[27] C. L. Bracey, P. R. Ellis, G. J. Hutchings, *Chem. Soc. Rev.* **2009**, *38*, 2231.
[28] S. Najafishirtari, R. Brescia, P. Guardia, S. Marras, L. Manna, M. Colombo, *ACS Catal.* **2015**, *5*, 2154.

[29] X. Li, S. S. S. Fang, J. Teo, Y. L. Foo, A. Borgna, M. Lin, Z. Zhong, *ACS Catal.* **2012**, *2*, 360.
[30] L. Zhang, H. Y. Kim, G. Henkelman, *J. Phys. Chem. Lett.* **2013**, *4*, 2943.
[31] D. Zhao, X. Xiong, C.-L. Qu, N. Zhang, *J. Phys. Chem. C* **2014**, *118*, 19007.
[32] M. Hajfathalian, K. D. Gilroy, A. Yaghoubzade, A. Sundar, T. Tan, R. A. Hughes, S. Neretina, *J. Phys. Chem. C* **2015**, *119*, 17308.
[33] S. Belin, C. L. Bracey, V. Briois, P. R. Ellis, G. J. Hutchings, T. I. Hyde, G. Sankar, *Catal. Sci. Technol.* **2013**, *3*, 2944.
[34] A. Sandoval, C. Louis, R. Zanella, *Appl. Catal., B* **2013**, *140*, 363.
[35] S. Yang, J. Chai, Y. Song, J. Fan, T. Chen, S. Wang, H. Yu, X. Li, M. Zhu, *J. Am. Chem. Soc.* **2017**, *139*, 5668.
[36] H. Yamamoto, H. Yano, H. Kouchi, Y. Obora, R. Arakawa, H. Kawasaki, *Nanoscale* **2012**, *4*, 4148.
[37] P. Wand, E. Kratzer, U. Heiz, M. Cokoja, M. Tschurl, *Catal. Commun.* **2017**, *100*, 85.
[38] H. Tsunoyama, N. Ichikuni, H. Sakurai, T. Tsukuda, *J. Am. Chem. Soc.* **2009**, *131*, 7086.
[39] M. Sadakiyo, M. Heima, T. Yamamoto, S. Matsumura, M. Matsuura, S. Sugimoto, K. Kato, M. Takata, M. Yamauchi, *Dalton Trans.* **2015**, *44*, 15764.
[40] S. Suzuki, Y. Tomita, S. Kuwabata, T. Torimoto, *Dalton Trans.* **2015**, *44*, 4186.
[41] R. Ferrando, J. Jellinek, R. L. Johnston, *Chem. Rev.* **2008**, *108*, 845.
[42] J. L. Rao, G. K. Chaitanya, S. Basavaraja, K. Bhanuprakash, A. Venkataramana, *J. Mol. Struct.: THEOCHEM* **2007**, *803*, 89.
[43] V. Ozoli, C. Wolverton, A. Zunger, *Phys. Rev. B* **1998**, *57*, 6427.
[44] A. R. Denton, N. W. Ashcroft, *Phys. Rev. A* **1991**, *43*, 3161.
[45] F. Yin, Z. W. Wang, R. E. Palmer, *J. Am. Chem. Soc.* **2011**, *133*, 10325.
[46] Z. Hai, N. El Kolli, J. Chen, H. Remita, *New J. Chem.* **2014**, *38*, 5279.
[47] B. Pauwels, G. Van Tendeloo, E. Zhurkin, M. Hou, G. Verschoren, L. T. Kuhn, W. Bouwen, P. Lievens, *Phys. Rev. B* **2001**, *63*, 165406.
[48] H. Yasuda, H. Mori, *Zeitschrift Phys. D Atoms, Mol. Clusters* **1996**, *37*, 181.
[49] S. Chen, S. V. Jenkins, J. Tao, Y. Zhu, J. Chen, *J. Phys. Chem. C* **2013**, *117*, 8924.
[50] S. J. Mejía-Rosales, C. Fernández-Navarro, E. Pérez-Tijerina, D. A. Blom, L. F. Allard, M. José-Yacamán, *J. Phys. Chem. C* **2007**, *111*, 1256.
[51] Z. W. Wang, R. E. Palmer, *J. Phys: Conf. Ser.* **2012**, *371*, 012010.
[52] K. Layek, M. Kantam, M. Shirai, D. Nishio-Hamane, T. Sasaki, H. Maheswaran, *Green Chem.* **2012**, *14*, 3164.
[53] E. Menumerov, R. A. Hughes, S. Neretina, *Nano Lett.* **2016**, *16*, 7791.
[54] Q. Zhang, D. A. Blom, H. Wang, *Chem. Mater.* **2014**, *26*, 5131.
[55] B. von Issendorff, R. E. Palmer, *Rev. Sci. Instrum.* **1999**, *70*, 4497.
[56] S. Saha, A. Pal, S. Kundu, S. Basu, T. Pal, *Langmuir* **2010**, *26*, 2885.